Research Article | Vol. 26, No. 7 | 2 Apr 2018 | OPTICS EXPRESS 7899
Optics EXPRESS

Time-domain characteristics of ultrafast transverse mode switching based on Si nanowires

YUAN YAN,[1] JIAMIN WANG,[1] HAOFAN YANG,[1] YUNTIAN CHEN,[1,2] YUN XIAO,[3] JING XU,[1,2,*] YU YU,[2] AND XINLIANG ZHANG[1,2]

[1]*School of Optical and Electronic Information, Huazhong University of Science and Technology, Wuhan, China*
[2]*Wuhan National Laboratory for Optoelectronics, Huazhong University of Science and Technology, Wuhan, China*
[3]*Wuhan Maritime Communication Research Institute, Wuhan, China*
[*]*jing_xu@hust.edu.cn*

Abstract: We investigate the potential of an ultrafast transverse mode switch based on silicon on insulator (SOI) platform for the switching applications in the spatial division multiplexing (SDM) systems. The impact of waveguide geometry, operation wavelength, pulse width of the pump and probe waves, as well as the temporal delay between the pulses are discussed with a special focus on the temporal switching windows of the switch. The optimized switching performances are further applied to a switching node in a hybrid optical time division-multiplexing (OTDM) and SDM system. The switching energy of the Si-based switch is shown to be potentially smaller than that of the Si_3N_4 based integration platform.

OCIS codes: (190.4223) Nonlinear wave mixing; (250.5300) Photonic integrated circuits; (060.2330) Fiber optics communications; (060.4230) Multiplexing.

References and links

1. R. Ryf, S. Randel, A. H. Gnauck, C. Bolle, R. Essiambre, P. Winzer, D. W. Peckham, A. McCurdy, and R. Lingle, "Space-division multiplexing over 10 km of three-mode fiber using coherent 6 × 6 MIMO processing," in *Optical Fiber Communication Conference/National Fiber Optic Engineers Conference* 2011, OSA Technical Digest (CD) (Optical Society of America, 2011), paper PDPB10.
2. A. Li, A. Al Amin, X. Chen, and W. Shieh, "Reception of mode and polarization multiplexed 107-Gb/s CO-OFDM signal over a two-mode fiber," in *Optical Fiber Communication Conference/National Fiber Optic Engineers Conference* 2011, OSA Technical Digest (CD) (Optical Society of America, 2011), paper PDPB8.
3. D. J. Richardson, J. M. Fini, and L. E. Nelson, "Space-division multiplexing in optical fibres," Nat. Photonics **7**(5), 354–362 (2013).
4. D. Dai, J. Wang, and Y. Shi, "Silicon mode (de)multiplexer enabling high capacity photonic networks-on-chip with a single-wavelength-carrier light," Opt. Lett. **38**(9), 1422–1424 (2013).
5. C. Koebele, M. Salsi, D. Sperti, P. Tran, P. Brindel, H. Mardoyan, S. Bigo, A. Boutin, F. Verluise, P. Sillard, M. Astruc, L. Provost, F. Cerou, and G. Charlet, "Two mode transmission at 2×100 Gb/s, over 40 km-long prototype few-mode fiber, using LCOS-based programmable mode multiplexer and demultiplexer," Opt. Express **19**(17), 16593–16600 (2011).
6. D. I. Kroushkov, G. Rademacher, and K. Petermann, "Cross mode modulation in multimode fibers," Opt. Lett. **38**(10), 1642–1644 (2013).
7. M. Schnack, T. Hellwig, and C. Fallnich, "Ultrafast, all-optical control of modal phases in a few-mode fiber for all-optical switching," Opt. Lett. **41**(23), 5588–5591 (2016).
8. R. Essiambre, M. A. Mestre, R. Ryf, A. H. Gnauck, R. W. Tkach, A. R. Chraplyvy, Y. Sun, X. Jiang, and R. Lingle, "Experimental investigation of inter-modal four-wave mixing in few-mode fibers," IEEE Photonics Technol. Lett. **25**(6), 539–542 (2013).
9. J. Xu, G. S. Gordon, T. Wilkinson, and C. Peucheret, "Experimental observation of non-linear mode conversion in few-mode fiber," presented at *Conference on Lasers and Electro-Optics (CLEO)*, OSA Technical Digest (online) (Optical Society of America, 2015), paper SM2L.3.
10. L. Rishøj, P. Kristensen, S. Ramachandran, and K. Rottwitt, "Experimental demonstration of intermodal nonlinear effects between full vectorial modes in a few moded fiber," Opt. Express **21**(23), 28836–28841 (2013).
11. K. Uesaka, K. K.-Y. Wong, M. E. Marhic, and L. G. Kazovsky, "Wavelength exchange in a highly nonlinear dispersion-shifted fiber: theory and experiments," J. Sel. Top. Quantum Electron. **8**(3), 560–568 (2002).

#318062 https://doi.org/10.1364/OE.26.007899
Journal © 2018 Received 20 Dec 2017; revised 3 Mar 2018; accepted 5 Mar 2018; published 19 Mar 2018

Optics EXPRESS

12. R. C. Youngquist, J. L. Brooks, and H. J. Shaw, "Two-mode fiber modal coupler," Opt. Lett. **9**(5), 177–179 (1984).
13. D. Dai, Y. Tang, and J. E. Bowers, "Mode conversion in tapered submicron silicon ridge optical waveguides," Opt. Express **20**(12), 13425–13439 (2012).
14. N. Andermahr and C. Fallnich, "Optically induced long-period fiber gratings for guided mode conversion in few-mode fibers," Opt. Express **18**(5), 4411–4416 (2010).
15. T. Hellwig, M. Schnack, T. Walbaum, S. Dobner, and C. Fallnich, "Experimental realization of femtosecond transverse mode conversion using optically induced transient long-period gratings," Opt. Express **22**(21), 24951–24958 (2014).
16. T. Hellwig, J. P. Epping, M. Schnack, K.-J. Boller, and C. Fallnich, "Ultrafast, low-power, all-optical switching via birefringent phase-matched transverse mode conversion in integrated waveguides," Opt. Express **23**(15), 19189–19201 (2015).
17. A. Gajda, L. Zimmermann, M. Jazayerifar, G. Winzer, H. Tian, R. Elschner, T. Richter, C. Schubert, B. Tillack, and K. Petermann, "Highly efficient CW parametric conversion at 1550 nm in SOI waveguides by reverse biased p-i-n junction," Opt. Express **20**(12), 13100–13107 (2012).
18. F. Poletti and P. Horak, "Description of ultrashort pulse propagation in multimode optical fibers," J. Opt. Soc. Am. B **25**(10), 1645–1654 (2008).
19. Y. Ding, J. Xu, H. Ou, and C. Peucheret, "Mode-selective wavelength conversion based on four-wave mixing in a multimode silicon waveguide," Opt. Express **22**(1), 127–135 (2014).
20. S. A. Miller, M. Yu, X. Ji, A. G. Griffith, J. Cardenas, A. L. Gaeta, and M. Lipson, "Low-loss silicon platform for broadband mid-infrared photonics," Optica **4**(7), 707–712 (2017).
21. K. Debnath, H. Arimoto, M. K. Husain, A. Prasmusinto, A. Al-Attili, R. Petra, H. M. H. Chong, G. T. Reed, and S. Saito, "Low-loss silicon waveguides and grating couplers fabricated using anisotropic wet etching technique," Front. Mater. **3**, 10 (2016).
22. J. Wang, S. He, and D. Dai, "On-chip silicon 8-channel hybrid (de)multiplexer enabling simultaneous mode- and polarization-division-multiplexing," Laser Photonics Rev. **8**(2), L18–L22 (2014).

1. Introduction

The interest in utilizing transverse modes for information channels has been renewed since 2011 [1–3] due to the fiber capacity crunch foreseen by the community [4]. Wide efforts have been made to construct enabling components and subsystems towards spatial division multiplexing (SDM) transmission systems that explore the orthogonality of the transverse mode sets in optical waveguides. With such endeavor, a great deal of devices that could independently and accurately address the transverse modes of optical waveguides have emerged [1, 2, 4, 5], which offers exciting possibilities for exploiting fundamental inter-modal nonlinear optical effects in fibers or integrated waveguides [6–10]. On the other hand, the inter-modal nonlinearities among multiple transverse modes can be harvested to realize optical switches for amplification [10] or routing [3] applications in SDM systems. Kerr effects, which are induced by the third-order susceptibility $\chi^{(3)}$ of the optical waveguides, have been widely used as optical switching mechanism in single mode fiber systems, such as self-phase modulation, cross-phase modulation, four-wave mixing (FWM) etc. FWM Bragg scattering (FWM-BS) is a particular type of FWM where photons are exchanged between two pump waves (red arrows) as well as between the probe and idler waves (black arrows), as shown in Fig. 1(a). FWM-BS has been widely used for data exchange operations between two wavelength-division multiplexed (WDM) channels when they are configured as the probe and idler waves, respectively [11]. In order to meet the requirement of the energy and momentum conservation, $w_4 - w_3 = w_2 - w_1$ and $\beta_4 - \beta_3 = \beta_2 - \beta_1$ must be satisfied. By analogy, FWM-BS can be extended into multimode scenario, resulting in data exchange between modes (referred to as mode exchange in the following), where up to four different transverse modes are involved. Note that in contrast to static mode conversion realized by grating structures [12] or tapered waveguides [13] etc., such mode exchange is optically induced so that it can be inherently used as a mode switch. As shown in Fig. 1(b), multimode FWM-BS among four transverse modes of a nonlinear waveguide, i.e. quasi-TE0, TE1, TM0, and TM1 modes, is illustrated. Pump waves at the TE0 and the TE1 modes (both at frequency w_3) form a transient index grating that travels along the pump waves through multimode interference and Kerr effect. Probe wave at the TM0 (TM1) mode could be scattered into the TM1 (TM0)

Optics EXPRESS

mode (both at frequency w_1) if $\Delta\beta_{TE} = \beta_{TE0} - \beta_{TE1} = \Delta\beta_{TM} = \beta_{TM0} - \beta_{TM1}$, i.e., the difference between the propagation constants of the TE0 and the TE1 modes equals that of the TM0 and TM1 modes. In this case, energy conservation is satisfied automatically since $w_1 = w_2$ and $w_3 = w_4$ is established. In contrast to FWM-BS in single mode case where the idler is generated at a different wavelength, multimode FWM-BS may create scattering between the probe wave and the idler wave at the same wavelength due to waveguide birefringence. Therefore, the wavelength of the mode exchange operation can be preserved. This is favored in SDM switching nodes since different modes may share the same wavelength. As multimode FWM-BS describes a phenomenon that a particular transverse mode of the waveguide is switched to another transverse mode dynamically and is inherently ultrafast because it is Kerr effect, we use nomenclature ultrafast transverse mode switching instead of multimode FWM-BS in the rest of this work.

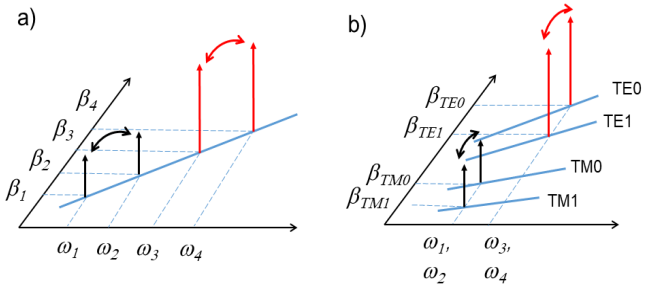

Fig. 1. Schematic diagrams of the phase matching condition of four-wave mixing Bragg scattering among four wavelengths in a single mode (a) and four transverse modes in two wavelengths (b).

Several works have been focused on ultrafast transverse mode switching, including fiber and integrated Si_3N_4 waveguide. By employing ultrashort pump pulses, switching energy has been reduced from 70 μJ [14] to 120 nJ [15] in few-mode fibers, and is expected to be further reduced from 120 nJ to 900 pJ in integrated Si_3N_4 waveguide [16]. Silicon-on-insulator (SOI), on the other hand, has been widely used as photonic integration platform since it is fully compatible with the Complementary Metal Oxide Semiconductor (CMOS) technology. In addition, silicon has even higher nonlinear-index coefficient n_2 and smaller effective mode volume A_{eff} than these of the Si_3N_4, which may enable even lower switching energy. Nevertheless, the advantage of stronger mode confinement may come at the cost of increased group velocity mismatch which may limit the effective interaction length of the ultrafast transverse mode switching. Nonlinear absorption associated with silicon is also detrimental to nonlinear effects, but may be relieved by using reverse biased PIN structures [17]. In this work, we investigate the ultrafast transverse mode switching in a multimode silicon waveguide by numerically modeling the pulse propagation in multimode waveguide and solving the multimode Schrodinger equation according to [18]. We show that by using pump pulses as short as 2 ps and 30 W peak power at each pump wave, i.e., switching energy of 120 pJ in total, it is possible to switch the power between the probe and idler waves with up to 90% efficiency.

In Section 2, we provide selection rules for the waveguide geometry as well as the pump and probe wavelengths. An SOI waveguide with cross section of 220 nm × 1250 nm and top silica cladding has been chosen for the rest of the study according to the boundary condition of C-band operation and group-velocity mismatch parameter. In section 3, temporal switching windows formed by two pulsed pump waves and a continuous-wave (CW) probe are investigated. A special focus is given to the group-velocity mismatch since four transverse modes are involved, which is degraded heavily compared to that of the single mode case. Since there exist two choices for pump waves (i.e., both in the TE or the TM modes) as well

Optics EXPRESS

as two choices for the probe wave (i.e., TX0 or TX1, "X" stands for "E" or "M"), four different cases can be derived and an optimum switching scenario can be found by comparing the temporal profile of the switching windows. In section 4, switching analysis for the optimum switching scenario is extended to the situation where a pulsed probe wave is used instead of a CW probe light. It is shown that the pulse width of the probe wave and the temporal delay among the pump waves and the probe wave can be optimized to facilitate over 90% conversion efficiency. In section 5, the optimized switching parameters are utilized to perform switching operation in a hybrid 160 Gbps optical time-division multiplexing (OTDM) and SDM system. The paper concludes in section 6.

2. Selection of waveguide geometry and operation wavelengths

The schematic diagram of the ultrafast transverse mode switching is shown in Fig. 2(a) using integrated photonic circuits, as described in [16]. The mode multiplexer (MUX) and demultiplexer (DEMUX) required in this scheme have been reported in several literatures [4, 19], which are out of the scope of this work. The multimode nonlinear waveguide considered in this work is a silicon strip waveguide, etched from an SOI wafer, and then deposited with a silica cladding layer on top, as shown in Fig. 2(b). Silicon layer with thickness h = 220 nm is a common value available for SOI wafers. Therefore, h is fixed as 220 nm throughout this work.

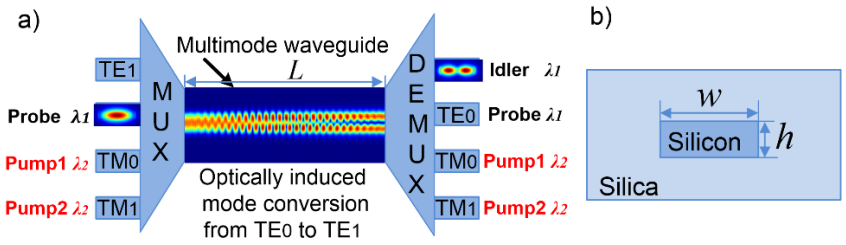

Fig. 2. (a) Schematic diagram of ultrafast transverse mode switching used for optically induced mode conversion. Four modes TE0, TE1, TM0 and TM1 are coupled to the multimode nonlinear waveguide through a mode multiplexer (MUX). Two pumps at the TM0 and the TM1 mode form an optical long period grating (OLPG) by multimode interference and Kerr effect in the multimode waveguide. The OLPG scatters the probe light on the TE0 mode to the idler light on the TE1 mode, which can be extracted by a mode de-multiplexer (DEMUX). (b) The cross-section of multimode silicon strip waveguide explored for ultrafast transverse mode switching.

To illustrate the rule of phase matching, Fig. 3(a) shows the value of $\Delta\beta_{TE}$ and $\Delta\beta_{TM}$ as a function of wavelength. The width of the waveguide in this case is 1250 nm. It is obvious that the intersection points that any horizontal lines go cross the line of $\Delta\beta_{TE}$ and $\Delta\beta_{TM}$ indicate the operation wavelength of the TE and the TM modes, respectively. For example, the operation wavelengths of the TE and the TM modes can be chosen at 1536 and 1552 nm, respectively, as shown by the dash-dotted line in Fig. 3(a). Therefore, for each TE wavelength it is possible to find a corresponding TM wavelength. Figure 3(b) shows the matched wavelength of the TM modes as a function of the wavelength of the TE modes for seven different waveguide widths. Note that TM modes are always assigned with the same wavelength, so are the TE modes, as illustrated in Fig. 1(b). The most common wavelength ranges used in optical fiber communication is 1530-1565 nm (C-band), which is the effective operation bandwidth of the erbium-doped fiber amplifier (EDFA). Therefore, we restrict the selection of wavelengths of both TE and TM modes in this range, as shown by the red dashed lines in Fig. 3(b). Except for the flexibility, group-velocity mismatch is another important factor when considering the selection of waveguide width since four transverse modes are involved. Therefore, we investigate the walk-off variance, σ_{GD}, defined according to [16],

Optics EXPRESS

$$\sigma_{GD} = \frac{1}{n-1}\sum_{i=1}^{n=4}\left|\beta_{1,i} - \overline{\beta_1}\right|^2)^{\frac{1}{2}} \quad (1)$$

for matched wavelength combinations for seven different w, as shown in Fig. 3(c) where red lines indicate that the operation wavelengths of both TE and TM modes are within the C-band. In the expression above, subscript 1 represents the first-order dispersion coefficient, which is the inverse of the group velocity, and subscripting i represents one of the four modes. $\overline{\beta_1}$ is the average of first-order dispersions of the four modes. It can be seen that the minimum σ_{GD} of a given w varies with w. The minimum achievable σ_{GD} is roughly the same for w ranging from 1250 nm to 1310 nm. Note that waveguides with smaller cross sections are favored in nonlinear applications due to the associated smaller effective mode volumes. Therefore, w = 1250 nm is chosen in this work for further study. Although the minimum σ_{GD} for w = 1250 nm at a wavelength combination of 1542 nm (TE) and 1570 nm (TM) is about 0.38 ps, the wavelength combinations in our work is chosen to be 1536 nm and 1552 nm, to make the two wavelengths in the C-band more flexible in real applications, resulting 0.03 ps/mm derivation from the optimum value.

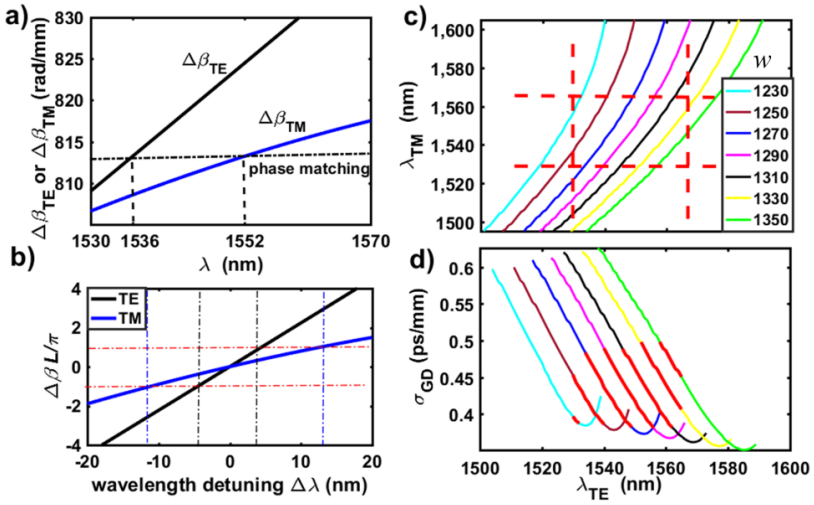

Fig. 3. (a) $\Delta\beta_{TE}$ (black) and $\Delta\beta_{TM}$ (blue) as a function of wavelength. The dash-dotted line indicates the case when $\Delta\beta = \Delta\beta_{TE} - \Delta\beta_{TM} = 0$. The operation wavelength of the TE and TM modes can be decided accordingly to be 1536 nm and 1552 nm, respectively. (b) The matched wavelength of the TM modes as a function of the wavelength of the TE modes, according to the phase matching condition when seven different waveguide widths (in nm unit) are considered. The red dashed lines enclose an area where both wavelengths are in the C band. (c) The standard deviation of the group delays per unit length of the four involved modes as a function of the TE wavelength. The bold red lines indicate that the wavelengths of the TE mode and the corresponding TM wavelengths are in the C band. (d) $\Delta\beta L/\pi$ as a function wavelength detuning for the TE (black) and the TM (blue) modes. w = 1250 nm and h = 220 nm is used in Fig. 3(a) and 3(d).

The operation bandwidth of the ultrafast transverse mode switching is also analyzed. The bandwidth of the scheme may be different depends on the choice of pump modes. When setting the TM modes as the pump modes, the operation bandwidth of the TE modes is obtained by fixing the TM wavelength at 1552 nm and calculating the range of wavelength detuning of the TE modes with respect to 1536 nm by the relation of $\Delta\beta L/\pi \le \pm 1$, where $\Delta\beta = \Delta\beta_{TE} - \Delta\beta_{TM}$, as shown by the black line in Fig. 3(d). L is the length of the waveguide

Optics EXPRESS

and is chosen to be unit length (1 mm) for a rough estimation of the bandwidth of the switch. L will be carefully optimized in the next section. The bandwidth of the TM mode can be obtained similarly. The operation bandwidth is estimated to be 7 and 24 nm, or 0.9 and 3 THz, for the TE and the TM mode, respectively, which would roughly support pulsed operation for pulse width larger than 1.1 ps and 0.33 ps (reciprocal of the bandwidth), respectively.

3. Temporal analysis of the switching window

In this section, we analyze the temporal profile of the switching window of two pulsed pump waves and a CW probe wave for silicon strip waveguide with a cross section of 220 nm × 1250 nm. The wavelengths of the TE and the TM mode are at 1536 nm and 1552 nm, respectively. Since different modes can be assigned to pump, probe as well as idler waves, four different situations occur, as shown in Fig. 4(a). The waveform of the probe wave at the output of the waveguide is a direct measurement of the temporal profile of the switching

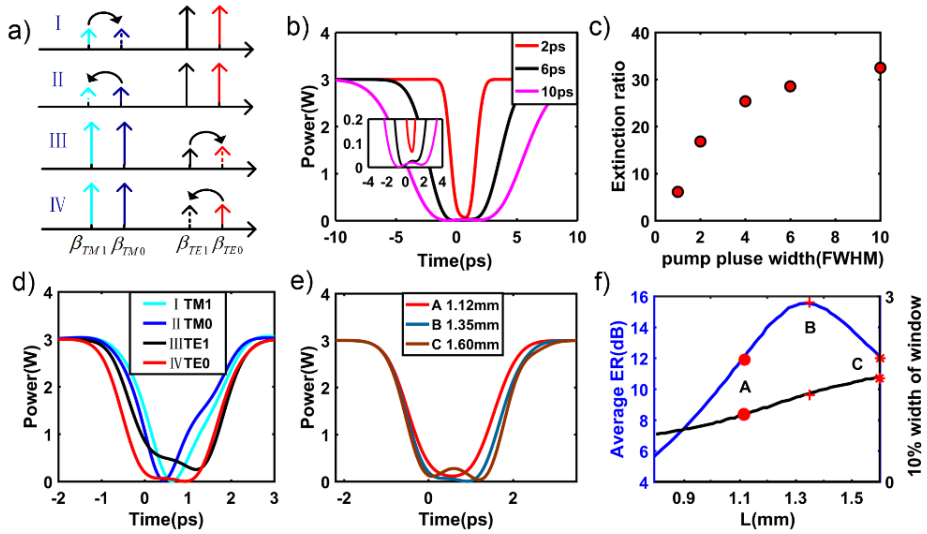

Fig. 4. (a) Four types of ultrafast transverse mode switching scenarios. (b) Switching window of type IV when the full-width-half-maximum of pump pulse is 2 ps (red), 6 ps (black) and 10 ps (magenta). L = 1.12 mm. (c) The extinction ratio of the switching window of type IV as a function of pump pulse width. (d) The switching window of four cases when the pulse width of the pump light is 2 ps. L = 1.12 mm. (e) The switching window of type IV at L = 1.12 mm (red), 1.35 mm (green) and 1.6 mm (brown). (f) The average extinction ratio of the switching window (blue) as well as the 10% of the width of the switching window (black) as a function of L. Marker A-C corresponds to the case shown in Fig. 4(e). Peak power of the pump and probe pulses is 30 W and 3 W in Fig. 4, respectively. Other parameters are the same as used in Fig. 3.

Table 1. Performances of the Four Types of the Switching Windows

Type	I	II	III	IV
Probe mode	TM_1	TM_0	TE_1	TE_0
10%Width (ps)	0.54	0.49	1.13	1.11
Average ER (dB)	13.3	12.5	10.5	12.4
σ_{3GD}(ps)	0.4	0.49	0.45	0.2

Optics EXPRESS

Table 2. Basic Parameters of the Four Transverse Modes

Wavelength	1552 nm		1536 nm	
Probe mode	TM_1	TM_0	TE_1	TE_0
β_1(ps/mm)	13.5	13.1	13.4	12.6
β_2 (ps^2/m)	16.9	12.4	–0.391	1.39
A_{eff} (μm^2)	0.09	0.1	0.19	0.18

window. Gaussian pulses are used throughout this work. Figure 4(b) shows the switching window of type IV for three different full-width-half-maximum (FWHM) pulse widths of the pump waves, i.e. 10 ps (magenta), 6 ps (black) and 2 ps (red). It is estimated from the continuous wave (CW) simulation where all waves are CW light that L could be on the order of millimeters when the peak power is on the order of tens of watts. For ease of calculation, we choose the peak power of the pump pulses to be 30 W and the resulting coupling length for full power transfer is 1.12 mm. Therefore, L = 1.12 mm is used in Fig. 4(b). The power of CW probe is chosen to be 3 W, which is 10% of the pump power, to avoid strong nonlinear effects induced by the probe wave. The inset shows a close look of the switching window around complete power transfer region. It can be seen that the extinction ratio of the switching window gets worse as the pulse width of the pump decreases from 10 ps to 2 ps due to the walk-off effect. Figure 4(c) shows the maximum extinction ratio (ER) of the switching window as a function of the pump pulse width, defined as the lowest point divided by the maximum point of the switching window. It can be seen that the ER drops below 20 dB as the pulse width approaches 2 ps, which is close to the bandwidth estimation in the last section for the TE mode, i.e. ~1.1 ps. We further examine the switching windows of the four switching types under 2 ps pump pulses, as shown in Fig. 4(d). Other parameters are the same as those used in Fig. 4(b). It can be seen that the profiles of the switching windows differ from each other significantly. Among the four cases, the switching window of type IV is the most regular and wide open with high ER. In order to better evaluate the performance of the switching windows, we introduce two parameters: 10% width of switching window and average ER estimated over the 10% window width. The 10% width of switching window is defined as the width at 10% of the highest point of the switching window, which is used to guarantee a larger width at the bottom of the switching window. The average ER is then defined as

$$average\ ER = \int_{10\%\ width} \frac{P_{\max}}{P(t)} dt \tag{1}$$

The average ER and the 10% width of these four modes are summarized in Table 1. It can be seen that the widths of type IV is about twice as large as that of type I and II and the average ER of type IV is close to type I and II. To explain this, let us first look at the β_1 parameter of four modes, as listed in Table 2. For the TM types, the TE modes are used as pump waves. According to Table 2, the TE1 pump pulse and the TE0 pump pulse walk off roughly 0.9 ps for L = 1.12 mm. Note that probe light is CW so that the walk off effect induced by the probe light can be ignored. On the contrary, TM1 pump pulse and TM0 pump pulse walk off about 0.45 ps for the TE switching types, which is about half of the value of the TM types. Note that although the probe wave is CW, the generated idler is also pulsed. Therefore, we propose an average walk off variance that takes the pump waves as well as the idler wave into account as

$$\sigma_{3GD} = \frac{1}{n-1} \sum_{i=1}^{n=3} \left| \beta_{1,i} - \overline{\beta_1} \right|^2)^{\frac{1}{2}} \tag{2}$$

Optics EXPRESS

where i represent the four waves involved in ultrafast transverse mode switching except the probe wave. The calculated σ_{3GD} for four switching types is shown in Table 1. It can be seen that the σ_{3GD} of type IV is the smallest among the four cases. This agrees with the fact that type IV has the best overall performance among the four situations. We further look at the switching performance of type IV with different L. Figure 4(e) shows the switching window at other two different L, i.e. 1.35 mm (green), and 1.6 mm (brown), where L = 1.12 mm (red) also shown for reference. When we increase the length of the waveguide, the performance is improved. This is because the power of the pump pulses is reduced due to the walk-off effect, resulting in increased coupling length. Figure 4(f) shows the 10% width and average ER as a function of L. Three cases shown in Fig. 4(e) are marked in Fig. 4(f) accordingly. It can be seen that the width of the switching window increases monotonically as L increases. On the other hand, the average ER increases until its maximum point at L = 1.35 mm and drops afterwards. Therefore, trade-off must be made between average ER and 10% width of switching window for L>1.35 mm. If high ER is not required, we can choose the waveguide at L = 1.6 mm. Considering the facts that 1.35 mm waveguide has the highest extinction ratio and relative narrow switching window, L = 1.35 mm is selected in the following work. The chromatic dispersion parameter β_2 of each mode is also shown in Table 2. The minimum dispersion length, calculated according to $T_0^2/|\beta_2|$, using $T_0 = 2/1.665 = 1.2$ ps, is about 85 mm, which is much longer than the waveguide length considered in this work, where the impact of chromatic dispersion can be neglected.

4. All-pulse switching dynamics

In the previous section, we mainly studied the performance of the switching window of CW probe light and improved the performance by optimizing the length of the waveguide. In this section, we investigate the switching of type IV under pulsed probe light since it has the best switching performance according to the analysis of last section. Figure 5(a) shows the temporal profiles of the switching window (red dotted line), probe pulse at the input (red solid line) and output (purple line) of the waveguide, where the pulse widths of the pump and the probe are 2 ps and temporally overlapped. By comparing the input waveform of the probe wave to the temporal shape of the switching window, it can be found that the center of the switching window is misaligned to that of the probe wave. This can be explained by the fact that the pump lights on the TM modes are moving faster than the probe light, according to Table 2, resulting in a large amount of residual power in the output of the probe wave. The conversion efficiency, η, defined as the energy ratio between the converted light, i.e. the idler light, and the energy of the input probe light, is lower than 70% in this case. In Fig. 5(b), the pump pulses are delayed to the probe pulse at the input of the waveguide by 0.64 ps. Clearly, the residual power in the output of the probe wave has been greatly reduced and the conversion efficiency is increased to about 80%. By further reducing the probe pulse width to 1ps and increasing the delay to 0.72 ps, as shown in Fig. 5(c), the residual power in the output of the probe wave is further reduced, leading to a conversion efficiency exceeding 90%. Figure 5(d) shows contour plot of the conversion efficiency as a function of the pulse width of the probe wave and the delay of the pump pulses to the probe pulse. The marker a, b, and c corresponds to the situation shown in Fig. 5(a), 5(b) and 5(c), respectively. It can be seen that by properly reducing the probe pulse width and adjusting the temporal alignment of the pump and the probe wave, it is possible to greatly increase the conversion efficiency. Note that the fringe of output probe pulse no longer matches well with that of the switching window in Fig. 5(c), in contrast to the case shown in Fig. 5(a) and 5(b). Due to the pulse width getting narrower, the spectrum of the probe light becomes broader, resulting in worse phase matching conditions. Since 1 ps width is already at the edge of the bandwidth limitation of the switch, as discussed in section 2, we believe phase-mismatch is the main contribution to such disagreement.

Optics EXPRESS

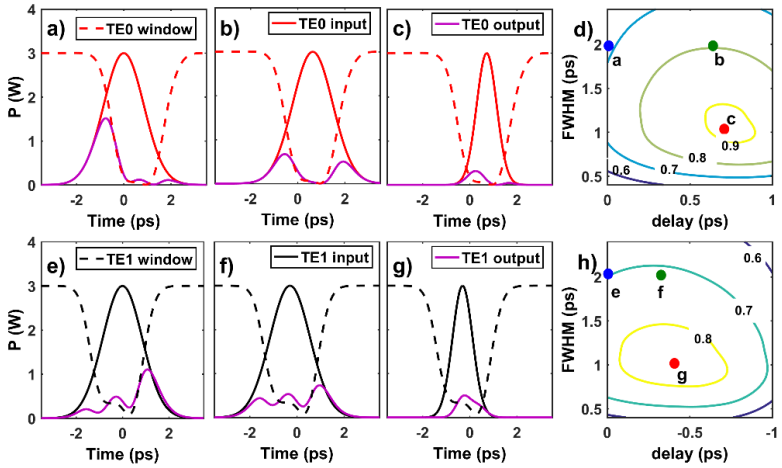

Fig. 5. The relationship between the switching window (dashed curve), input (red solid curve in (a)-(c) and black solid curve in (e)-(g)) and output of the probe light (purple). L = 1.35 mm. (a-c) The probe light is launched on the TE0 mode (type IV). (e-f) The probe light is launched on the TE1 mode (type III). (a), (e) Pump and probe pulses are temporally overlapped and all the pulse widths are 2ps. (b) The pump is delayed by 0.64 ps to the probe. Pulse widths are not changed. (c) Pump is delayed by 0.72 ps to the probe. The pulse width of the probe is reduced to 1 ps. (f) Probe is delayed by 0.39 ps to the pump pulses. Pulse widths are 2 ps. (g) Probe is delayed by 0.42 ps to the pumps. Pulse width of the probe is reduced to 1 ps. Contour plot of the conversion efficiency as a function of delay of the pump pulses and pulse width (probe) is given in Fig. 5(d) for type IV and in Fig. 5(h) for type III. Markers correspond to the case shown in Fig. 5(a)-5(c) and Fig. 5(e)-5(g). Other parameters are the same as used in Fig. 4.

We also look into the all pulse switching performance of type III since in the mode exchange application the energy is not only converted from the TE0 mode to the TE1 mode, but also from the TE1 mode to the TE0 mode. As shown in Fig. 5(e)-4(g), the black dotted curves are the switching window of type III switching. The black solid and purple waveforms in Fig. 5(e)-4(g) are the input and output of the probe waves, respectively. The pump and probe pulses are aligned at the input of the waveguide in Fig. 5(e) while probe pulses are delayed 0.39 ps to the pump pulses at the input of the waveguide in Fig. 5(f). Since the difference of the group velocity of the TE1, TM1 and TM0 mode is much smaller than that of the TE0, TM1 and TM0 mode, the conversion efficiency shown in Fig. 5(e) does not improve obviously. By delaying the probe pulse to the pump pulses by 0.42 ps and compressing the probe pulse to 1 ps width in Fig. 5(g), the conversion efficiency is increased from 70% to 84%, providing the potential for ultra-fast mode exchange. Figure 5(h) shows the contour plot of type III switching, similar to Fig. 5(d). Note that the final optimization conversion efficiency of the type IV switching exceeds 91%, which is better than that of the type III switching. This is in consistency with the analysis of the switching windows, as discussed in section 3.

It should be noted that the linear transmission losses of the silicon waveguide are not included in the previous analyses. Typical losses of single mode silicon waveguide can be made to ~1 dB/cm [20]. With advanced manufacturing process, silicon waveguides with even lower losses have been reported [21]. For multimode silicon waveguide discussed in the work, losses could be lower than that of the single mode waveguide due to a better mode confinement [22]. For the optimum working waveguide length of 1.35 mm founded in section 3, the transmission losses of the waveguide are less than 0.2 dB using 1 dB/cm loss value, which are very small. To better understand the impact of linear transmission losses, the conversion efficieny of type IV and III under the same condition as shown in Fig. 5(c) and 5(g), respectively, are reconsidered using losses of 1 dB/cm and 4 dB/cm for all the modes. The conversion efficiency (η) are summarized in Table 3. The conversion efficiencies of the

Optics EXPRESS

two types under 1 dB/cm degrade slightly from the case of no losses but drop significantly in the case of 4 dB/cm. Therefore, the impact of linear transmission losses on the performances of switching windows are moderate up to 1 dB/cm, which is achievable under the state of art technology.

Table 3. Conversion Efficiency of Type III and IV with Loss of 0, 1 and 4 dB/cm

Loss (dB/cm)	0	1	4
η (Type III)(%)	83.6	78.2	70
η (Type IV)(%)	90.7	87.3	77.6

5. Application of mode switching in OTDM + SDM system

In this section, we apply the ultrafast transverse mode switching to realize the add-drop functionality in optical time division multiplexing (OTDM) system when combined with SDM technologies, as shown in Fig. 6(a). The SOI photonic integrated circuit shown in Fig. 2(a) can be used as the optical add-drop multiplexing (OADM) switching node, where a 160 Gbps OTDM data stream is loaded on the TE1 mode (signal 1), and a 10 Gbps OTDM tributary (signal 2) is loaded on the TE0 mode. Signal 2 is aligned to a specific OTDM channel of signal 1. Take channel 1 for example. By launching 10 GHz pump pulses on the TM1 and TM0 mode and make the pump pulses aligned with channel 1 of signal 1, it is possible to switch the data between channel 1 of signal 1 and signal 2. That is, using such a switch, it is possible to

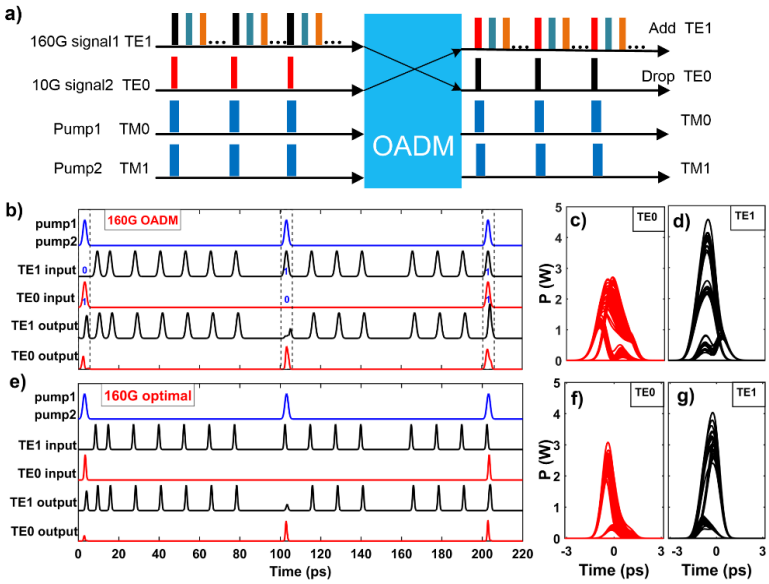

Fig. 6. (a) Schematic diagram of applying the ultrafast transverse mode switching in the OADM switching node in a hybrid OTDM + SDM system. (b) The temporal waveforms of the 10 GHz pump, signal 1 (160 Gbps) and signal 2 (10 Gbps) at the input and the output of the waveguide. All the pulse widths are 2 ps and temporally overlapped. The peak power of the pump and signals pulses are 30 W and 3 W, respectively. L = 1.35 mm. (c), (d) Eye diagrams of the output TE0 and TE1 modes. (e) Optimal switching results by reducing the signal pulse width to 1 ps and shifting the signals pulses according to the parameters given in section 4. (f)(g) The optimized eye diagram of the output TE0 and TE1 modes. Loss = 0 dB/cm.

download a 10 Gbps signal from a high-speed 160 Gbps signal in the TE0 mode, and simultaneously upload a 10 Gbps signal to a high-speed 160 Gbps in the TE1 mode. Note that such mode switching operation is wavelength preserving. Loss is set to zero in this section according to the discussion in section 5.

Optics EXPRESS

As shown in Fig. 6(b), two pump lights are modulated with a 10 GHz periodic signal, and the pulse width is 2 ps. The 160 Gbps and 10 Gbps signals, both with 2 ps pulse width, are launched in the TE1 and TE0 mode, respectively. Under the control of the pump light, the signals on the two modes are switched. There are four kinds of information exchange, but only three of them need to be considered: data "0" in the TE0 mode, "1" in the TE1 mode; "1" in the TE0 mode, "0" in the TE1 mode; "1" in the TE0 mode, "1" in the TE1 mode (defined as case 1-3). Clearly, case 1 and 2 corresponds to type III and IV switching, respectively. The pump pulses and the probe pulses are temporally overlapped. For case 1, the conversion efficiency of type IV is not satisfactory, which may introduce error bits in the add channel. For case 2, the peak power of residual energy in the TE0 mode is too high, which may lead to the generation of error bits for the drop channel. For the case 3, the peak power of the TE1 mode is higher than that of the TE0 mode, since the switching performance of type IV is better than that of type III. Figure 6(c) and 6(d) show the eye diagrams of the TE0 mode and the TE1 mode at the output of the switch, where the eyes are not well opened.

Next, we optimize the OADM switching performance by applying the parameters derived in the previous section. The signal 1 and 2 are both reduced to 1 ps pulse width, meanwhile, signal 1 is delayed by 0.72 ps to the pump pulses and signal 2 is shifted ahead of the pump pulses by 0.42 ps in Fig. 6(e). In Fig. 6(f) and 6(g), the eye diagrams of the TE0 mode and the TE1 mode have been greatly improved. The average switching power in this case is ~1.2 W (30.8 dBm), which is beyond two-photon absorption (TPA) threshold of the silicon and can be greatly reduced by using a reverse biased PIN junction [17].

6. Conclusion

In conclusion, we investigate an ultrafast transverse mode switch with low pump power and high conversion efficiency based on SOI nanowires by modeling conversion process with multi-mode coupled nonlinear Schrodinger equations. By tailoring the geometry of the silicon nanowire, it is possible to operate the switch in the C-band wavelength region with THz bandwidth. It is shown that the Si switch features much lower switching energy compared to that of the Si_3N_4 due to a combination of larger nonlinear-index coefficient n_2, smaller effective mode volume A_{eff}, moderate group-velocity mismatch and negligible chromatic dispersion. The switching bandwidth as well as the switching energy of this work is limited by the walk-off effect, i.e. group-velocity mismatch. The degree of waveguide height freedom has not been investigated and may be a good parameter to improve the wave-off performance of the switch. Note that the ultimate limitation of the bandwidth and energy of the ultrafast transverse mode switching mechanism will be the phase matching and losses, respectively. By carefully optimize the waveguide length, pulse width and the temporal delay between the pump and probe pulses, it is possible to achieve a conversion efficiency over 90% without resorting to the help of reducing the waveguide length, resulting in a switching energy of 120 pJ, which is more than seven fold smaller than that reported in [16]. The usage of the switch is further considered in a hybrid OTDM + SDM switching scenario, where a high-speed 160 Gps OTDM signal is considered. Wide open eye diagrams are shown to be possible using the optimized ultrafast transverse mode switch under an average switching power of 30.8 dBm, where the Si waveguides must be equipped with reverse biased PIN structures in order to remove the detrimental carrier effects. Note that Si waveguides without PIN structures may be used when the switching repetition rate is reduced. Since the SDM technology is widely explored to overcome the capacity crunch of single optical fibers, we expect this work offers guidelines for the design of ultrafast SDM switches based on the SOI platform.

Funding

Natural National Science Foundation of China (NSFC) (61405066, 61405067, 61775063 and 61735006); National Key Research and Development Program of China (2017YFA0305200).